Structure of the phage TP901-1 1.8 MDa baseplate suggests an alternative host adhesion mechanism

David Veesler[a,b,1,2], Silvia Spinelli[a,b], Jennifer Mahony[c], Julie Lichière[a,b], Stéphanie Blangy[a,b], Gérard Bricogne[d], Pierre Legrand[e], Miguel Ortiz-Lombardia[a,b], Valérie Campanacci[a,b,3], Douwe van Sinderen[c,f], and Christian Cambillau[a,b,1]

[a]Architecture et Fonction des Macromolécules Biologiques, Aix-Marseille Université, Campus de Luminy, Case 932, 13288 Marseille Cedex 09, France; [b]Architecture et Fonction des Macromolécules Biologiques, Centre National de la Recherche Scientifique, Unité Mixte de Recherche 6098, Campus de Luminy, Case 932, 13288 Marseille Cedex 09, France; [c]Department of Microbiology, University College Cork, Western Road, Cork, Ireland; [d]Global Phasing Ltd., Sheraton House, Castle Park, Cambridge CB3 0AX, United Kingdom; [e]Synchrotron Soleil, L'Orme des Merisiers Saint-Aubin - BP 48, 91192 Gif-sur-Yvette Cedex, France; and [f]Alimentary Pharmabiotic Center, University College Cork, Cork, Ireland

Edited by* Michael G. Rossmann, Purdue University, West Lafayette, IN, and approved April 9, 2012 (received for review January 18, 2012)

Phages of the *Caudovirales* order possess a tail that recognizes the host and ensures genome delivery upon infection. The X-ray structure of the approximately 1.8 MDa host adsorption device (baseplate) from the lactococcal phage TP901-1 shows that the receptor-binding proteins are pointing in the direction of the host, suggesting that this organelle is in a conformation ready for host adhesion. This result is in marked contrast with the lactococcal phage p2 situation, whose baseplate is known to undergo huge conformational changes in the presence of Ca^{2+} to reach its active state. In vivo infection experiments confirmed these structural observations by demonstrating that Ca^{2+} ions are required for host adhesion among p2-like phages (936-species) but have no influence on TP901-1-like phages (P335-species). These data suggest that these two families rely on diverse adhesion strategies which may lead to different signaling for genome release.

bacteriophage | crystal structure | *Lactococcus lactis* | siphoviridae | viral infection

Bacterial viruses (phages) are elegant nanomachines infecting their hosts with high specificity and efficiency. The vast majority of them belong to the *Caudovirales* order and possess a tail appendage used to recognize the host and ensure genome delivery. This organelle seems to be responsible for the unequaled efficacy of these virions, as compared to eukaryotic viruses, as each phage particle can infect a target cell (1). The initial events of the infection process have been characterized for a limited number of phages demonstrating that dramatic conformational changes at the distal tail end accompany the DNA injection event (2–7). Binding of myophage T4 to the host lipopolysaccharides induces dramatic rearrangements of its tail extremity allowing irreversible commitment to the target cell followed by puncturing of its surface (3, 5). The emerging picture for *Podoviridae* is that after attachment to the cell envelope, the minor phage proteins are ejected to form a tube across the periplasm thereby directing the viral DNA into the host cytoplasm (8). Siphophage p2, belonging to the 936-species of lactococcal phages, exhibits a Ca^{2+}-mediated activation mechanism inducing a 200° rotation of the receptor-binding proteins (RBPs) to establish multiple interactions with host saccharides and initiate infection (7). Here we report the crystal structure of the baseplate from the lactococcal phage TP901-1 (P335-species) at 3.8 Å resolution and show that it is in a conformation ready for host adhesion, ruling out the involvement of a Ca^{2+}-mediated or any other major conformational changes of this organelle at this initial step. We extended these conclusions by demonstrating that authentic virions can infect their host with maximal efficacy in the absence of added Ca^{2+} and that this behavior is conserved among the TP901-1 phage species (P335). We therefore suggest that TP901-1-like phages do not rely on baseplate conformational changes for host adsorption, in contrast to what has been observed for phage p2 and all other long-tailed phages. We also suggest that these diverse mechanisms might have implications on the signaling of genome release.

Results

Structure Determination. *Siphoviridae* adsorption organelles (tail-tips or baseplates) are assembled from the gene products encoded at the end of the morphogenesis module (9) (Fig. 1). The phage TP901-1 baseplate is composed of a central core made of distal tail protein (Dit) and the tail fiber (Tal) as well as a double-disk peripheral structure encompassing the baseplate upper protein (BppU) and the RBP (BppL) (10). We overexpressed the virtually complete TP901-1 baseplate (Dit, BppU, and RBP) (11) and crystallized it, initially yielding poorly diffracting crystals improved through the use of an additive, dehydration and by tailoring the cryoprotection step. Phases were derived by combining a Ta multiwavelength anomalous diffraction (MAD) dataset with two mercury single-wavelength anomalous diffraction (SAD) datasets (Table S1) and by fitting the RBPs (10, 12) (Fig. S1*A*) and the SPP1 Dit hexamer (13, 14) (Fig. S1*B*) structures in the electron density. We were able to build a poly-Ala model for BppU therefore leading to a near-complete baseplate structure and sequence assignment was aided by solving the structure of the isolated BppU N-terminal domain (Fig. S1*C*) as well as of the BppU C-terminal domain in complex with the RBP (Fig. S1 *D–E*). The TP901-1 baseplate is 300 Å wide and 160 Å high, exhibiting an overall six-fold symmetry, and has a mass of 1.76 MDa (Fig. 1 *A–C*). From the proximal to distal end, it is formed by 18 copies of BppU arranged around a central Dit hexamer and holding 54 RBPs organized as 18 trimers (Fig. 1 *A–D*).

Structure of a 1.8 MDa Baseplate. The Dit protein forms a hexameric circular-shaped core of 80 Å(diameter) × 36 Å(height), which delineates a 37-Å wide central channel (Fig. 1 and Fig. 2 *A–B*). Six domains are evenly appended to the bottom of this core without making contact between each other (Fig. 2*A*). Each monomer

Author contributions: D.v.S. and C.C. designed research; D.V., S.S., J.M., J.L., S.B., P.L., M.O.-L., V.C., and C.C. performed research; G.B. and M.O.-L. contributed new reagents/analytic tools; D.V., S.S., J.M., G.B., V.C., D.v.S., and C.C. analyzed data; and D.V., D.v.S., and C.C. wrote the paper.

The authors declare no conflict of interest.

*This Direct Submission article had a prearranged editor.

Data deposition: Structure factors have been deposited in the Protein Data Bank, www.pdb.org [PDB ID codes 4DIV and 4DIW (baseplate), 3UH8 (BppU N-terminal domain), 3U6X (tripod)].

[1]To whom correspondence may be addressed. E-mail: cambillau@afmb.univ-mrs.fr or david.veesler@afmb.univ-mrs.fr.

[2]Present address: Department of Molecular Biology, The Scripps Research Institute, 10550 North Torrey Pines Road, La Jolla, CA 92037.

[3]Present address: Laboratoire d'Enzymologie et de Biochimie Structurales UPR 3082, Bâtiment 34, Avenue de la Terrasse, F-91198 Gif-sur-Yvette Cedex.

This article contains supporting information online at www.pnas.org/lookup/suppl/doi:10.1073/pnas.1200966109/-/DCSupplemental.

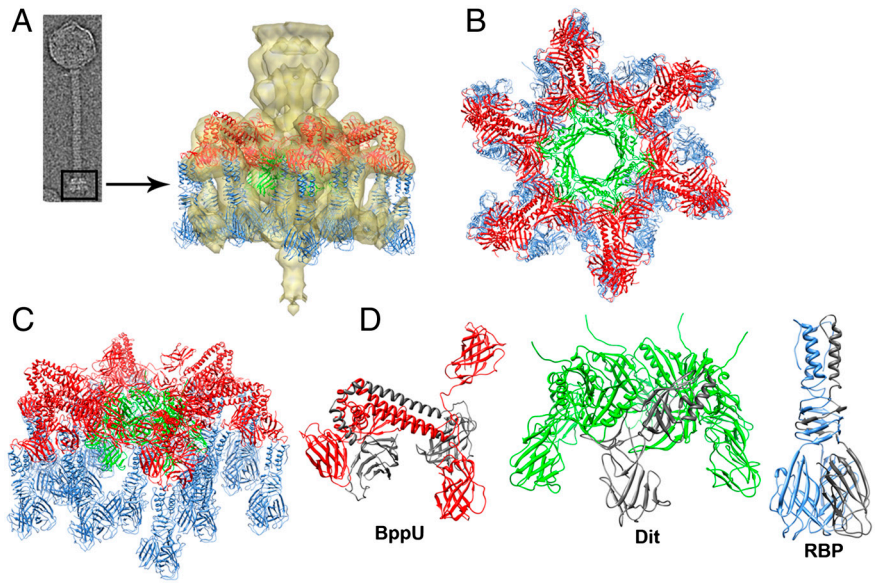

Fig. 1. Structure of the *L. lactis* phage TP901-1 baseplate (i.e., host adsorption machinery). (*A*, *Left*) Negative-stained electron micrograph of a TP901-1 virion. (*Right*) Close-up view of the phage baseplate X-ray structure fitted in the adsorption device three-dimensional electron microscopy reconstruction (the region is highlighted by a black square on the micrograph). The baseplate is formed by 18 copies of BppU (red) arranged around a central Dit hexamer (green) and holding eighteen trimeric RBPs (receptor-binding proteins, blue). (*B*) Top view of the baseplate looking down the phage tail tube axis. (*C*) Semitilted view of the baseplate rotated by 30° relative to *A*. (*D*) The three different types of polypeptides present in the organelle. (*Left*) A BppU trimer, (*Center*) the Dit hexamer, and (*Right*) a RBP trimer. One monomer within each protein homooligomer is depicted in dark gray.

comprises: (*i*) an N-terminal domain (residues 1–145) with a β-sandwich, an α-helix, and a β-hairpin; (*ii*) a C-terminal domain (residues 146–255) folded as a galectin-like β-sandwich (7, 14) (Fig. 1*D* and Fig. 2*A*). The six N-terminal domains form the Dit central core, with each β-hairpin projected toward the neighboring monomer to ensure the cohesion of the hexamer, whereas the six C-terminal domains account for the extension radiating from the ring. The Dit structure is strikingly similar to that of phages SPP1 (14) and p2 (7), substantiating the conservation of this module that forms the adsorption apparatus hub in phages of Gram+ bacteria (9) (Fig. S2). However, in phage p2 two Dit hexamers are present back-to-back with each galectin domain from the lower ring attaching a trimeric RBP to the baseplate via a specific extension (7) (Fig. S2).

The eighteen BppU assemble as six asymmetric trimers connecting the Dit central core and the RBPs (Fig. 1 *A–D*, Fig. 2 *A–C*, and Fig. 3*A*). Each monomer is composed of an N-terminal globular domain (1–122), a linker (123–134), two helices joined by a kink (135/139–194), and a globular C-terminal domain (195–299) (Fig. 3 *A–B*). The N-terminal domain exhibits a β-sandwich immunoglobulin fold resembling the plexin-A2 C-terminal domain [Fig. S3, Protein Data Bank (PDB) ID code 3OKY, DALI Z-score = 7.1; rmsd = 2.3 Å (15)]. Within each BppU trimer, the two innermost N-terminal domains (Nt1 and Nt2, Fig. 2*C* and Fig. 3*A*) contact the equivalent domains from flanking trimers yielding a 156-Å wide and 32-Å high crown-shaped dodecameric ring surrounding the Dit hexameric core (Fig. 2 *A–C*). The third N-terminal domain is laterally projected onto the long helices belonging to the adjacent BppU trimer (Fig. 2 *B–C* and Fig. 3*A*). As the three BppU N-terminal domains belonging to a given trimer harbor linkers differing in length and structure at their C termini, the three long helical segments are out-of-register relative to each other in term of amino-acid sequence (Fig. 3 *A–B*). These helices form an approximately 25° angle relative to the plane of the Dit ring (in direction of the capsid) and end by a kink whose length differ in each monomer allowing (with the length of the long helices) to achieve a sequence rephasing of the three chains. The three following short helices are pointing toward the distal tail extremity with a local threefold symmetry (Fig. 2*A*), before reaching the C-terminal domains folded as β-sandwiches (Fig. 2 *B–C* and Fig. S1*E*). These latter domains assemble as a threefold symmetric triangular-shaped trimer held via two types of antiparallel pairing (Fig. 2*A*, Fig. 3*A*, and Fig. S1*E*) and burying a surface of 240 $Å^2$ by monomer at each interface.

The RBP structure is identical to its isolated structure forming a trimer with three domains (10): (*i*) an N-terminal shoulder domain (residues 1–32) built from three extended loops and a three-helix bundle; (*ii*) a central triple β-helix neck domain (residues 33–62); and (*iii*) a C-terminal head domain assembled from three β-barrels (residues 63–163) defining three receptor-binding sites at their interface (Fig. 1*D*). The three RBPs within each tripod are separated by at least 20 Å (Fig. S4 *A–B*) whereas extensive intertripod contacts involving the twelve most internal RBPs are observed (Fig. S4*E*). Noteworthy, the six most peripheral RBPs do not establish any contact and appear to be highly mobile, as attested by their weak density in the baseplate EM reconstruction obtained from intact virions (10) (Fig. 1*A* and Fig. S5*A*). This observation is further supported by the RBP trimers conformation in the isolated tripod structure revealing that they can oscillate around their anchoring point (Fig. S4 *C–D*) whereas this freedom is only retained by the six most external ones in the whole baseplate (Fig. S4*E*).

Among the twelve BppU N-terminal domains surrounding the central Dit hexamer, six such moieties simultaneously contact the Dit N- and C-terminal domains of two different monomers whereas the other six interact with a single Dit N-terminal domain. Each BppU C-terminal domain deeply projects a loop (residues 217–234) in the crevice formed at the top of the RBP trimer to anchor it to the baseplate (Fig. 2*D*, *Left*). This interface is characterized by outstanding complementarity of shape (burying approximately 1,600 $Å^2$ of the RBP trimer surface) and electrostatic potential, as the negatively charged penetrating loop (Fig. 2*D*, *Lower Right*) fills the positively charged crevice (Fig. 2*D*, *Upper Right*). Moreover, three aliphatic/aromatic residues belonging to BppU (Ile 219, Phe 226, and Phe 232) fill the cup center of the RBP trimer. The conservation of the residues involved in the BppU/RBP interactions suggests that common architectural themes are found among P335-phages (Fig. 2 *E–F*).

Architecture of the TP901-1 Tail and Host Adsorption Apparatus. Our TP901-1 tail and baseplate EM reconstruction (10) allows proposing an atomic scale model for the components that make up these organelles (Fig. 1*A* and Fig. S5 *A–B*). The tail tube is formed of stacked major tail protein hexamers that can be modeled using the type six secretion system Hcp structure because of their high structural similarity (16, 17). The baseplate crystal structure reported here (Dit, BppU, and RBP) is nicely accommodated as a rigid body in the virion EM map and clearly matches the discernible features of the reconstruction. In agree-

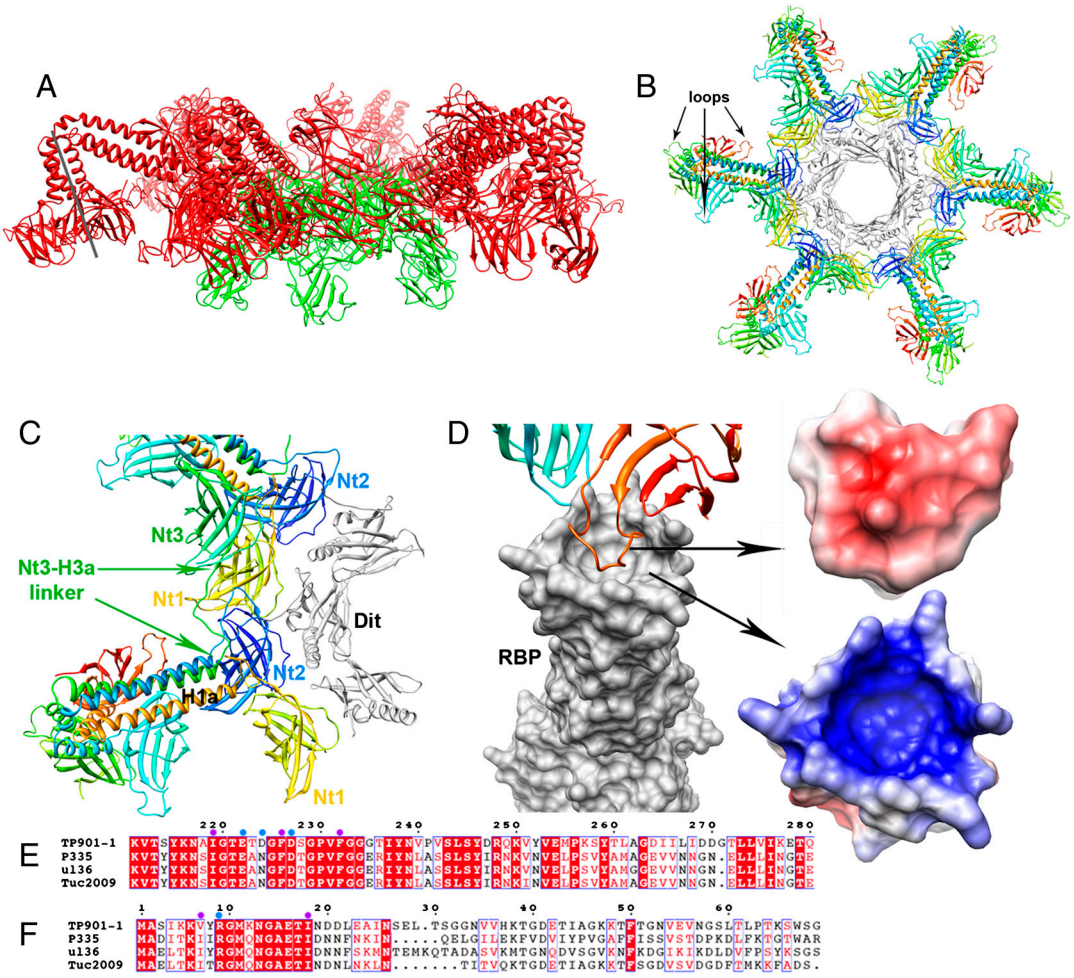

Fig. 2. Interactions between the different TP901-1 baseplate proteins. (*A*) The six BppU trimers (red) form a crown around the central Dit hexamer (green). The threefold symmetry axis present within the BppU small helical segments and C-terminal domains (residues 180–299) is evidenced for one BppU trimer. (*B*) Top view of the baseplate looking down the phage tail tube axis (the RBP trimers have been removed for clarity). Each BppU trimer exhibits an asymmetric organization emphasized through coloring the three nonequivalent BppU chains with a shade of blue, green, and red. The BppU N-terminal domain dodecameric ring surrounding Dit (depicted in light gray) is composed of the yellow (Nt1) and blue (Nt2) domains. (*C*) Close-up view of the interactions established between BppU and Dit (light gray). The three BppU N-terminal domains are labeled Nt1 to Nt3 with Nt1 and Nt2 forming the dodecameric ring whereas Nt3 interacts with the adjacent BppU trimer. Note the differences in both structure and length observed at the level of the linkers connecting Nt domains with the long helices. The Dit C-terminal domains have been removed for clarity. (*D*, *Left*) Each RBP trimer (light gray) is anchored to the baseplate via a loop extending from each BppU C-terminal domain (orange) that penetrates the cup formed at the top of this former protein. (*Right*) Close-up view of the electrostatic surface potential of the interacting regions from BppU (*Upper*) and the RBP (*Lower*) highlighting their high charge and surface complementarity. Multiple sequence alignments of BppU proteins (*E*) and RBPs (*F*) from phages TP901-1, P335, ul36, and Tuc2009. Only the region corresponding to the RBP-interacting loop (BppU residues 211–280) is shown. The conserved amino-acids involved in the interactions between the two proteins are indicated by a purple circle for aliphatic/aromatic residues or a blue circle for charged residues.

ment with our native mass spectrometry data (18), a single Dit hexamer is present in the virion and aligns its central channel with the tail tube one to form the DNA ejection conduit. Finally, we modeled the tail fiber (Tal) N-terminal domain using the (closed) p2 ORF16 trimer, which is expected to share a virtually identical fold (9).

Discussion

Molecular Basis of an Alternative Adhesion Mechanism. This work reports the second host adsorption device structure from a phage of *Lactococcus lactis* and reveals that the TP901-1 baseplate dramatically differs from that of phage p2 despite the conservation of their central core. The TP901-1 organelle mass exceeds by approximately 90% that of p2 (taking into account the tail fiber) and accommodates three times as many RBPs (54 instead of 18). The TP901-1 baseplate harbors its receptor-binding sites directed toward the distal extremity, i.e., in a direction compatible with instant host adhesion, suggesting that it is in a functionally active conformation. The overall rigidity of this structure, due to the reduced conformational freedom of its constituents, suggests that the baseplate is permanently ready-for-adhesion and does not rely on any triggering mechanism involving large protein motions. This mechanism is in marked contrast with the phage p2 baseplate whose RBPs undergo a 200° rotation (promoted/stabilized by Ca^{2+} ions present in the medium) to allow a tight binding to the host surface (7). We therefore investigated the effect of Ca^{2+} on the infectivity yield of lactococcal phages belonging to the 936-species (e.g., p2) and to the P335-species (e.g., TP901-1). Phage infection assays clearly demonstrated that 936-species bacteriophages are strictly dependent on Ca^{2+} for infectivity and in a concentration-dependent manner (Fig. 4*A* and Table S2). Conversely, P335-virions exhibit no Ca^{2+} dependency for infection with the exception of Tuc2009 showing a basal infection potential that can be enhanced proportionally to the Ca^{2+} concentration [the baseplate of this latter phage is known to have a different composition than that of TP901-1 (19)]. Superimposing

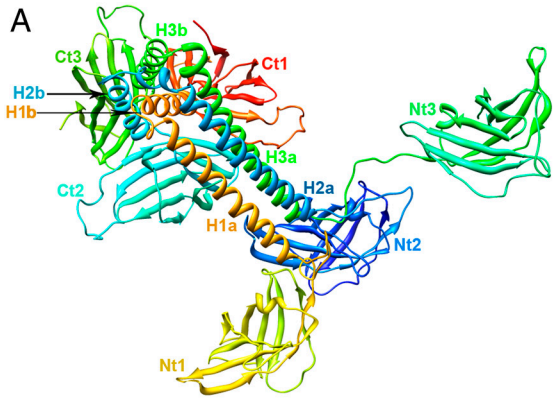

Fig. 3. The BppU (ORF48) structure. (*A*) One BppU trimer is depicted to emphasize on the kink responsible for rephasing of the amino acid residues between the three monomers. Each monomer is colored with a shade of blue, green, or red and the individual domains or segments are annotated. (*B*) The three BppU N-terminal domains belonging to a single trimer have been superimposed to highlight the difference in both structure and length between their linkers connecting to the long helices.

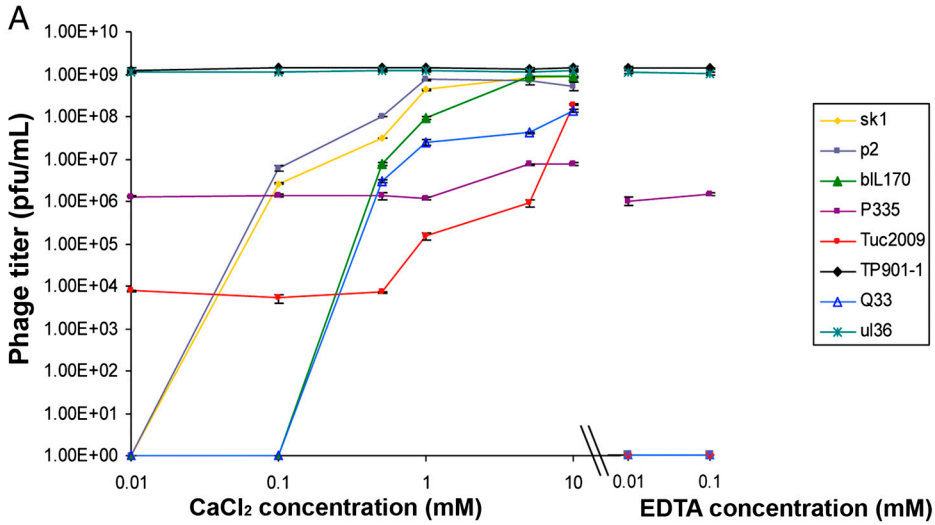

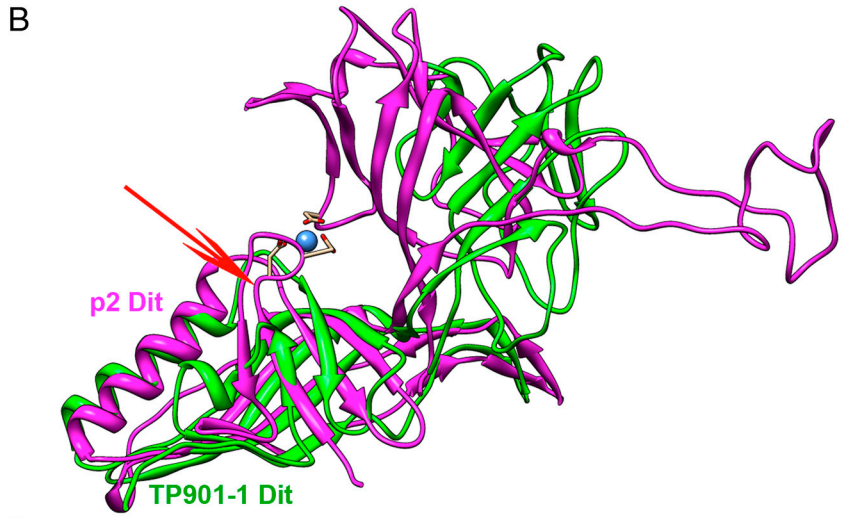

C

```
p2          ---------- ---------- MVRQYKIHTN LDGTDDKVWD VTNG----KV RFYQ-PSNL.
bIL170      ---------- ---------- MVRQYKIHTN LDGTDDKVWD VTNG----KV RFYQ-PSNL.
sk1         ---------- ---------- MVRQYKIHTN LDGTDDKVLD VTNG----KV RLYQ-PSNL.
TP901-1 MYKFRDTTKQ KHYRNLPFIP -TSAMSYD-- ------GAWL ---EELIEGY QTLAVE-GRE
P335    MYKFRDTTKQ KHYRNLPFIP -TSAMSYD-- ------GTWL ---EELIEGY QTLTVE-GRE
ul36    MYKFRDTTKQ EHYRNLPFIP -TSAMSYD-- ------GTWL ---EELIEDY QTLTVE-GRE
Tuc2009 MYKFRDTTKQ KHYRNLPFIP -TSAMSYD-- ------GTWL ---EELIEGY QTLTVE-GRE
```

Fig. 4. Effect of Ca^{2+} ions on lactococcal phages infectivity in vivo. (*A*) Phage titre [expressed as plaque-forming units per milliliter (pfu/mL)] for virions of the 936-species (p2, bIL170, and sk1) or P335-species (TP901-1, Tuc2009, P335, and ul36) in the presence of varying concentrations of Ca^{2+} ions. The phages from the 936 family strictly depend on this divalent cation for infectivity whereas P335-phages are fully infectious in the absence of such ions (with the exception of Tuc2009 that exhibits a partial infectivity in the absence of Ca^{2+} that could be explained by its different baseplate composition). (*B*) Superimposition of the Dit N-terminal domains of phages TP901-1 (green) and p2 (pink) showing the absence of the Ca^{2+} binding loop in this former phage (red arrow) and explaining the difference of phenotype between the two phage species (P335 and 936). (*C*) Structure-based sequence alignment of the Dit sequences from the 936 and P335 phages used in the in vivo assay based on the structural superimposition in *B*.

the N-terminal domain of the p2 and TP901-1 Dit structures reveals that the loop involved in Ca^{2+} binding in the former phage is absent in the latter one explaining the observed difference of behavior relative to this cation (Fig. 4*B*, red arrow). Furthermore, structure-based sequence alignment of Dit proteins from phages used in the infection assay demonstrates that this feature appears to be a hallmark distinguishing 936 and P335 species (Fig. 4*C*). Our in vivo results are in agreement and corroborated by the structural data confirming thus that TP901-1 and related P335-phages rely on a substantially different strategy for initiating infection compared to phages of the 936-species. This adhesion mechanism is unprecedented and dramatically different to what has been described for other long tailed viruses [such as T4 (1, 5)] as it does not rely on any major conformational transitions within the adsorption device.

Infection Mechanism and DNA Release Trigger in p2 and P335-Species Viruses. P335 and 936-virions interact only with saccharides of the *L. lactis* cell envelope during infection (7). We propose that TP901-1 adsorbs via its RBP head domains to the oligosaccharide phosphate repeating units forming the pellicle layer present at the surface of the host (Fig. S6) (12, 20–23), making thus the process irreversible because of the avidity of interactions (10, 24). We have previously formulated the hypothesis that the baseplate conformational changes observed in phage p2 might be involved in the cascade of events resulting in connector opening and DNA release (7) (as in the case of phage T4). Based on the data presented here along with the literature, it is tempting to speculate that TP901-1 only relies on subtle baseplate conformational changes for generating the firing signal at the onset of infection. TP901-1 Tal might interact with the pellicle and generate the DNA release signal through an initial mechanical stress. In this scenario, the events localized in the tail fiber might be the stimulus triggering the cascade of conserved conformational changes in the tail tube and the connector eventually resulting in DNA ejection (6, 25). Indeed, phages assembled in the absence of the tape measure protein (TMP, filling the tail tube channel before genome ejection) or Dit or the tail fiber are tailless (26, 27). This observation suggests that the TMP C-terminal domain and the tail fiber N-terminal domain directly interacts, constituting a likely pathway to propagate the signal for infection. This hypothesis is further supported by a recent work showing that the tail fiber is responsible for generating this signal in phage SPP1 (28). Alternatively, one can also envision that binding of several RBPs to the host receptors might result in subtle tripods mechanical distortions triggering the firing mechanism [in a way reminiscent of complement activation in the lectin pathway (29)] through BppU by communicating it directly to the most distal major tail protein (MTP) ring that is apposed onto Dit (Fig. S5*A*).

Materials and Methods

Crystallography. The TP901-1 baseplate was expressed and purified as described previously (11). Crystals were grown by hanging-drop vapor diffusion and all datasets were collected at synchrotrons Soleil (PROXIMA 1) and the European Synchrotron Radiation Facility (ID14.4). The structure was initially solved using experimental phase information before fitting atomic coordinates in the resulting electron-density maps.

Calcium Dependency Assay. Plaque assays were performed using an adapted version of the double-agar method (30).

ACKNOWLEDGMENTS. We are deeply grateful to J.E. Johnson for fruitful discussions and his interest in this work. We also thank synchrotrons Soleil (Saint-Aubin, France) and European Synchrotron Radiation Facility (ESRF) (Grenoble, France) for beamtime allocation. This work has been funded by the Agence Nationale de la Recherche Grants ANR BLAN07-1_191968 and ANR-11-BSV8-004-01; Ministère Français de l'Enseignement Supérieur et de la Recherche PhD Grant 22976-2006 (to D.V.); and Science Foundation Ireland Principal Investigator Award 08/IN.1/B1909 (to D.v.S.).

1. Kostyuchenko VA, et al. (2003) Three-dimensional structure of bacteriophage T4 baseplate. *Nat Struct Biol* 10:688–693.
2. Aksyuk AA, et al. (2009) The tail sheath structure of bacteriophage T4: A molecular machine for infecting bacteria. *EMBO J* 28:821–829.
3. Kanamaru S, et al. (2002) Structure of the cell-puncturing device of bacteriophage T4. *Nature* 415:553–557.
4. Kostyuchenko VA, et al. (2005) The tail structure of bacteriophage T4 and its mechanism of contraction. *Nat Struct Mol Biol* 12:810–813.
5. Leiman PG, Chipman PR, Kostyuchenko VA, Mesyanzhinov VV, Rossmann MG (2004) Three-dimensional rearrangement of proteins in the tail of bacteriophage T4 on infection of its host. *Cell* 118:419–429.
6. Plisson C, et al. (2007) Structure of bacteriophage SPP1 tail reveals trigger for DNA ejection. *EMBO J* 26:3720–3728.
7. Sciara G, et al. (2010) Structure of lactococcal phage p2 baseplate and its mechanism of activation. *Proc Natl Acad Sci USA* 107:6852–6857.
8. Chang JT, et al. (2010) Visualizing the structural changes of bacteriophage Epsilon15 and its salmonella host during infection. *J Mol Biol* 402:731–740.
9. Veesler D, Cambillau C (2011) A common evolutionary origin for tailed-bacteriophage functional modules and bacterial machineries. *Microbiol Mol Biol Rev* 75(3):423–433.
10. Bebeacua C, et al. (2010) Structure and molecular assignment of lactococcal phage TP901-1 baseplate. *J Biol Chem* 285:39079–39086.
11. Campanacci V, et al. (2010) Solution and electron microscopy characterization of lactococcal phage baseplates expressed in *Escherichia coli*. *J Struct Biol* 172:75–84.
12. Spinelli S, et al. (2006) Modular structure of the receptor binding proteins of *Lactococcus lactis* phages. The RBP structure of the temperate phage TP901-1. *J Biol Chem* 281:14256–14262.
13. Goulet A, et al. (2011) The opening of the SPP1 bacteriophage tail, a prevalent mechanism in gram-positive-infecting siphophages. *J Biol Chem* 286:25397–25405.
14. Veesler D, et al. (2010) Crystal structure of bacteriophage SPP1 distal tail protein (gp19.1): A baseplate hub paradigm in gram-positive infecting phages. *J Biol Chem* 285:36666–36673.
15. Holm L, Rosenstrom P (2010) Dali server: Conservation mapping in 3D. *Nucleic Acids Res* 38:W545–W549.
16. Pell LG, Kanelis V, Donaldson LW, Howell PL, Davidson AR (2009) The phage lambda major tail protein structure reveals a common evolution for long-tailed phages and the type VI bacterial secretion system. *Proc Natl Acad Sci USA* 106:4160–4165.
17. Leiman PG, et al. (2009) Type VI secretion apparatus and phage tail-associated protein complexes share a common evolutionary origin. *Proc Natl Acad Sci USA* 106:4154–4159.
18. Shepherd DA, Veesler D, Lichiere J, Ashcroft AE, Cambillau C (2011) Unraveling lactococcal phage baseplate assembly by mass spectrometry. *Mol Cell Proteomics* 10, 10.1074/mcp.M111.009787.
19. Sciara G, et al. (2008) A topological model of the baseplate of lactococcal phage Tuc2009. *J Biol Chem* 283:2716–2723.
20. Chapot-Chartier MP, et al. (2010) Cell surface of *Lactococcus lactis* is covered by a protective polysaccharide pellicle. *J Biol Chem* 285:10464–10471.
21. Ricagno S, et al. (2006) Crystal structure of the receptor-binding protein head domain from *Lactococcus lactis* phage bIL170. *J Virol* 80:9331–9335.
22. Spinelli S, et al. (2006) Lactococcal bacteriophage p2 receptor-binding protein structure suggests a common ancestor gene with bacterial and mammalian viruses. *Nat Struct Mol Biol* 13:85–89.
23. Tremblay DM, et al. (2006) Receptor-binding protein of *Lactococcus lactis* phages: Identification and characterization of the saccharide receptor-binding site. *J Bacteriol* 188:2400–2410.
24. Veesler D, et al. (2009) Crystal structure and function of a DARPin neutralizing inhibitor of lactococcal phage TP901-1: Comparison of DARPin and camelid VHH binding mode. *J Biol Chem* 284:30718–30726.
25. Lhuillier S, et al. (2009) Structure of bacteriophage SPP1 head-to-tail connection reveals mechanism for viral DNA gating. *Proc Natl Acad Sci USA* 106:8507–8512.
26. Mc Grath S, et al. (2006) Anatomy of a lactococcal phage tail. *J Bacteriol* 188:3972–3982.
27. Vegge CS, et al. (2005) Structural characterization and assembly of the distal tail structure of the temperate lactococcal bacteriophage TP901-1. *J Bacteriol* 187:4187–4197.
28. Vinga I, et al. (2012) Role of bacteriophage SPP1 tail spike protein gp21 on host cell receptor binding and trigger of phage DNA ejection. *Mol Microbiol* 83:289–303.
29. Wallis R (2007) Interactions between mannose-binding lectin and MASPs during complement activation by the lectin pathway. *Immunobiology* 212:289–299.
30. Lillehaug D (1997) An improved plaque assay for poor plaque-producing temperate lactococcal bacteriophages. *J Appl Microbiol* 83:85–90.